Supplementary Material

Multifunctional Amphiphilic Ionic Liquid Pathway to Create Water-Based Magnetic Fluids and Magnetically-Driven Mesoporous Silica

Jing Shen*[a], Wen He[b] and Tongwen Wang[b]

[a]Department of Applied Chemistry, College of Vocational Education, Yunnan Normal University, Kunming 650092, P. R. China. Email: shenjingbox0225@hotmail.com.

[b]College of Chemistry and Chemical Engineering, Yunnan Normal University, Kunming 650092, P. R. China.

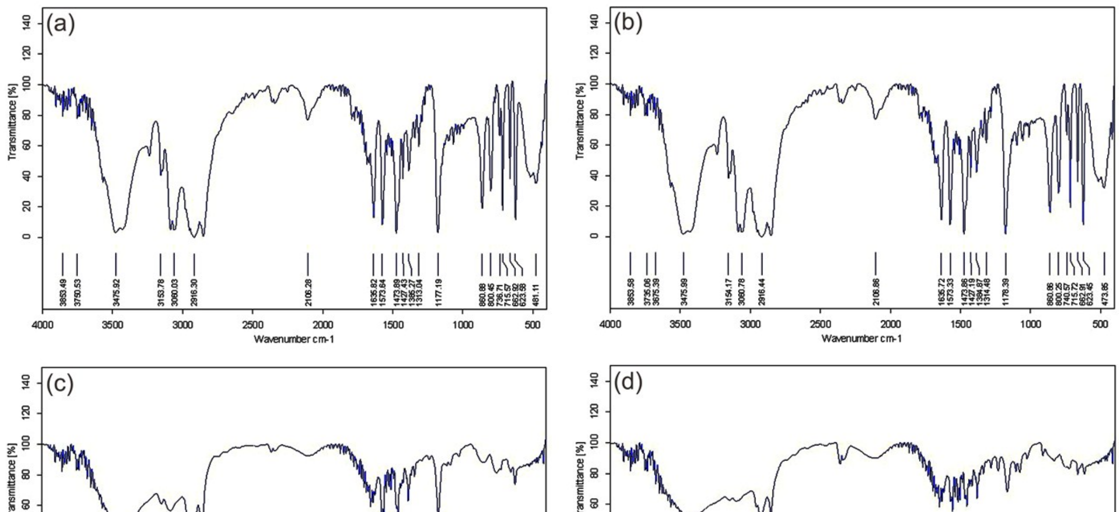

Fig. S1 IR spectrum of 1-alkyl-3-methylimidazolium chloride ($C_n$mimCl). *n* is the number of carbon atom in alkyl chain of ionic liquid, *n* = (a) 16, (b) 14, (c) 12 (d) 10, respectively.

Fig. S1 presents 1-alkyl-3-methylimidazolium chloride ($C_n$mimCl). *n* is the number of carbon atom in alkyl chain of ionic liquid, *n* = (a) 16, (b) 14, (c) 12 (d) 10, respectively. For the analysis of C_{16}mimCl (Fig. S1a), the bands at 3471 cm^{-1} and 3412 cm^{-1} can be attributed to the antisymmetric v_3 and symmetric v_1 stretching modes of water, where the water interacts with the anion via H-bonding in a symmetric complex $Cl^{-}\cdots H–O–H\cdots Cl^{-}$(ref. L. Cammarata, S. G. Kazarin, P. A. Salter and T. Welton, *Phys. Chem. Chem. Phys.* 2001, **3**, 5192.). Next to that, the two characteristic bands around 3155 cm^{-1} and 3142 cm^{-1}, which can be assigned to the symmetric ν_s CH(4, 5) and asymmetric ν_{as} CH(4, 5) stretch of in positions four and five of the imidazolium ring (ref. B. D. Fitchett, J. C. Conboy, *J. Phys. Chem.* 2004, **108**, 20255.). The peaks around 3060 cm^{-1} are contribution from the asymmetric stretching ν_{as} N-CH$_3$ of the methyl group bound to the imidazolium ring. The next strong bands at 2915 cm^{-1} and 2853 cm^{-1} can be assigned to the antisymmetric ν_{as} CH$_2$ and symmetric ν_s CH$_2$ stretching modes of the alkyl chain. The analysis of other vibration mode assignment can be seen in our early work.[26] Therefore, the results allow conclusion that the C_{16}mimCl with imidazolium ring and alkyl chain was synthesized. For other C_{14}mimCl (Fig. S1b), C_{12}mimCl (Fig. S1c) and C_{10}mimCl (Fig. S1d), analogous results can be obtained. However, the intensity of these peaks decreased with decreasing the value of *n*.

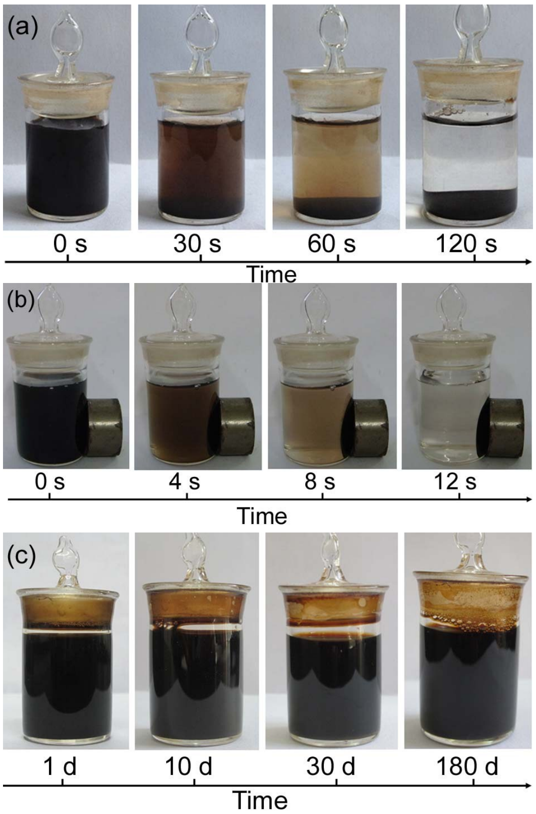

Fig. S2 Digital photographs of (a) natural sedimentation of Fe_3O_4/C_{10}mimCl, (b) magnetically separable state of Fe_3O_4/C_{10}mimCl and (c) Fe_3O_4/C_{10}mimCl/C_{16}mimCl dispersion at different time.

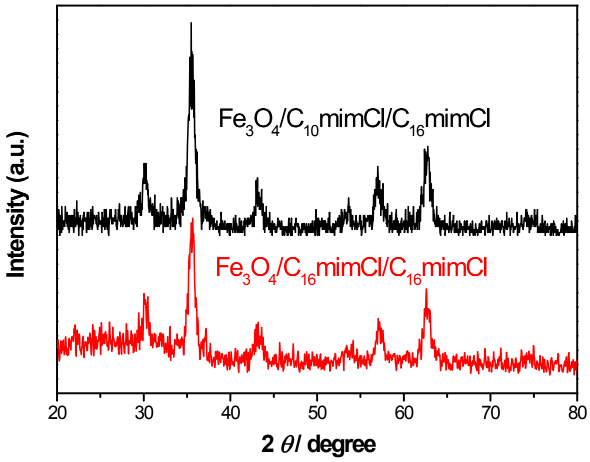

Fig. S3 Wide-angle XRD patterns of $Fe_3O_4/C_{10}mimCl/C_{16}mimCl$ and $Fe_3O_4/C_{16}mimCl/C_{16}mimCl$.

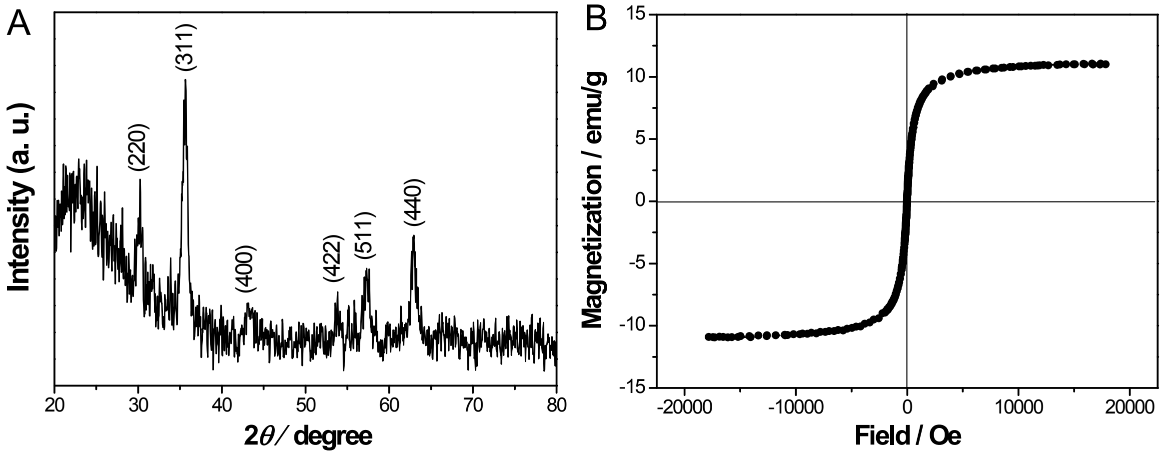

Fig. S4 (A) Wide-angle XRD pattern and (B) magnetization curve of calcined sample prepared using $C_{16}mimCl$ as template in the $Fe_3O_4/C_{16}mimCl/C_{16}mimCl$ magnetic fluid with an initial molar ratio $n(Fe_3O_4/C_{16}mimCl/C_{16}mimCl)/n(TEOS)$ of 0.05.

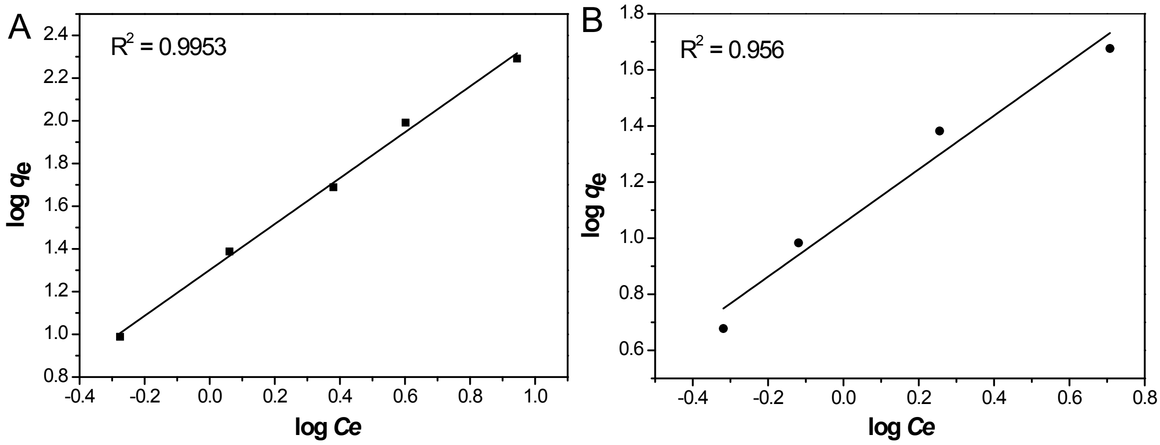

Fig. S5 Linear relation fitted by Freundlich isotherm equation for (A) RhB and (B) MB solutions adsorbed on Fe_3O_4/MCM-41.

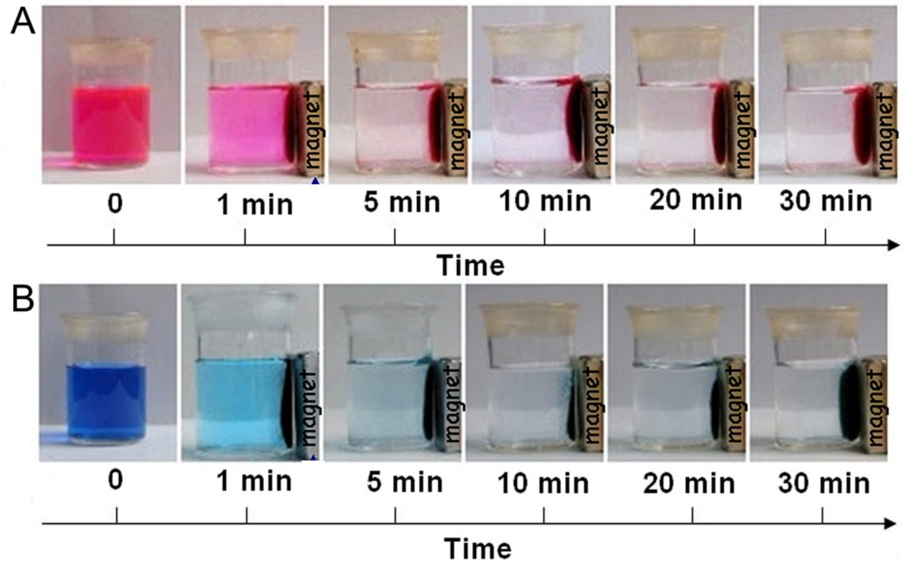

Fig. S6 Digital photographs of separated effect of (A) rhodamine B and (B) methylene blue solutions (100 mg L^{-1}) after adsorption on Fe_3O_4/MCM-41 at different time interval, and a permanent magnet was placed next to the solution.